Chin. J. Astron. Astrophys. Vol. 2 (2002), No. 3, 277–286
(*http://www.chjaa.org* or *http://chjaa.bao.ac.cn*)

Chinese Journal of Astronomy and Astrophysics

Line Broadening in a Limb Flare: Derivation of Macro-turbulent Velocity Fields

Ying Liu and Ming-De Ding ⋆

Department of Astronomy, Nanjing University, Nanjing 210093

Received 2002 January 20; accepted 2002 March 14

Abstract The line profiles of Hα in a limb flare on 1998 November 11 appear to be unusually broadened. It is considered that macro-turbulence (or macroscopic mass motions) may be one of the main causes. We use an inversion technique to extract the probability distribution of the line-of-sight velocity in the flare. There exist some differences between the velocity distributions deduced from Hα and from Ca II λ8542, which may be because the two lines depend differently on the temperature and velocity. Since the loop density is high, we obtain a rather short cooling time (several tens of seconds) from the hot X-ray loops to the cool loops visible in Hα. Possible origins of the large scale motions are discussed.

Key words: Sun: flares - Sun: atmospheric motions - Line: profiles

1 INTRODUCTION

Unusual line broadening during solar flaring events has been observed in different lines, such as the lines in soft X-ray spectra (e.g., Antonucci et al. 1982; Bentley et al. 1986), the He I λ10830 line (You et al. 1998), and the Hα line (e.g., Graeter & Kucera 1992). All these events exhibit a common feature: the line width significantly exceeds the thermal Doppler width, which cannot be explained by a Doppler broadening mechanism or a pure Stark effect (You & Oertel 1992). Ding et al. (1999) reported another event. The flare (importance SF/C3.2) occurred at N25W86 on 1998 November 11 and was observed simultaneously in Hα and Ca II λ8542 with an imaging spectrograph in the solar tower of Nanjing University (Huang et al. 1995). The flare began at 02:10 UT, reached its maximum at 02:15 UT, and ended at 02:18 UT. Figure 1 displays the typical line profiles of Hα and Ca II λ8542 at 02:14:38 UT at the three locations, denoted by A, B and C in the flaring loop (see fig. 1 in Ding et al. 2002). From Fig. 1, we can see that the line profiles are extraordinarily broadened, and the Hα profile is the broadest near the top of the flaring loop. This broadening lasted a rather long time and extended into the later phase of the flare.

This unusual line broadening implies some physical processes that are important to the understanding of flaring phenomena. Ding et al. (1999) showed that the line opacity effect cannot fully account for the observed line width of Hα. Fang et al. (2000) examined the effect

⋆ E-mail: dmd@nju.edu.cn

of non-thermal excitation and ionization by an electron beam, and found that the Hα line can become very broad at an altitude where the source function reaches its radial maximum. However, this may not be the main broadening mechanism, since the unusual broadening in this event extended into the later phase when the non-thermal effect does not take a leading role in the formation of lines. Li & You (2001) proposed that an expanding atmosphere can explain the unusually broad profile of the He I λ10830 line in a limb flare on 1989 August 16. They obtained an empirical velocity distribution which represents one of the possibilities that could occur.

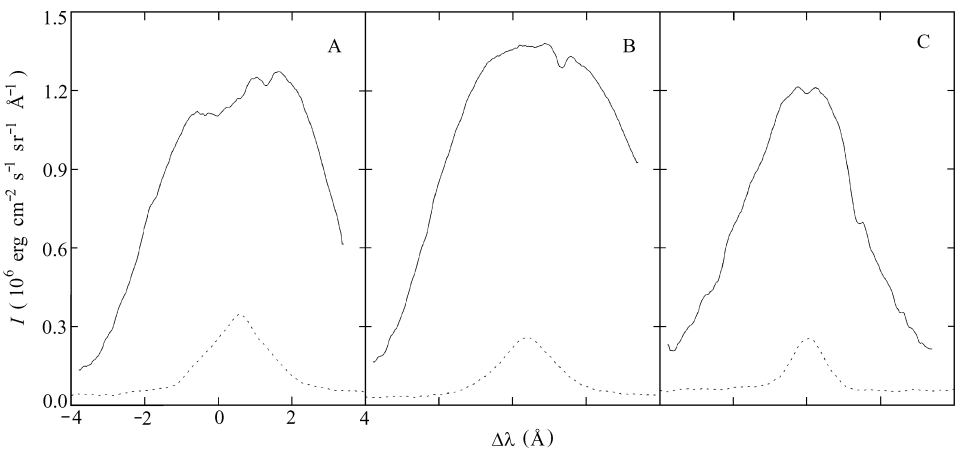

Fig. 1 Line profiles of Hα (solid lines) and Ca II λ8542 (dotted lines) at 02:14:38 UT corresponding to the three locations indicated in Ding et al. (2002). Location B is at the top of the loop, while locations A and C are in the legs.

In solar flares, various mass motions can occur such as due to the untwisting or squeezing of magnetic structures, or due to the gas dynamics in the flaring loop. Recent observations have indeed reported large scale radial or horizontal motions (e.g., Malherbe et al. 1997; You et al. 1998), the velocity of which can reach more than 160 km s^{-1}. Emslie & Alexander (1987) showed that all of the excess line broadening observed in the solar disk could be explained by the superposition of many hydrodynamic motions within flaring loops. Gu et al. (1984) proposed that the plasma within a helical structure of the magnetic field would spiral downward under certain conditions; some authors (e.g., Heinzel et al. 1992) pointed out that large line broadening of unknown origin could be ascribed to such rotational motions. Raju (1998) further demonstrated that mass motions within coronal loops can lead to line broadening observed at the limb. It is thus natural to relate the unusual broadening of line profiles in the limb flare on 1998 November 11 to such large inhomogeneous mass motions. In this work, we will extract the probability distribution of the velocity field along the line of sight in the flaring loop, examine its role in the line broadening and discuss its origin.

2 METHOD OF COMPUTATION

As mentioned in Sect. 1, mass motion in flaring loops represents a significant factor in the understanding of the line broadening. It is thus indispensable to determine the velocity

distribution. Newton et al. (1995) used a continuous Gaussian fitting to derive the velocity distribution from soft X-ray spectra. Following their idea, we develop a method to treat the Hα and Ca II λ8542 lines. We propose that many macro-turbulent elements (i.e., fine structures) are confined in a spatially unresolved region, and these elements can be regarded as radiatively disconnected; every element moves with a different velocity along the line of sight. Assuming that the emission from all the turbulent elements has the same profile except for different Doppler shifts, the observed line profile can be expressed as

$$I(\Delta\lambda) = \int i(\Delta\lambda - \frac{v\lambda_0}{c}) P(v) \mathrm{d}v \,, \tag{1}$$

where $P(v)$ is the velocity probability distribution, λ_0 is the line center wavelength, and $i(\Delta\lambda - \frac{v\lambda_0}{c})$ is the line intensity from a turbulent element with velocity v. For a homogeneous element $i(\Delta\lambda)$ is given by

$$i(\Delta\lambda) = S[1 - e^{-\tau(\Delta\lambda)}] \,, \tag{2}$$

where the source function S is assumed to be constant and wavelength independent. The optical thickness is given by

$$\tau(\Delta\lambda) = \tau_0 H(a, x) \,, \tag{3}$$

where τ_0 is the optical thickness at line center, and $H(a, x)$ is the Voigt profile, defined as

$$H(a, x) = \frac{a}{\pi} \int_{-\infty}^{+\infty} \frac{e^{-y^2}}{a^2 + (x - y)^2} \mathrm{d}y \,, \tag{4}$$

where

$$x = \frac{\Delta\lambda}{\Delta\lambda_\mathrm{D}} \,, \tag{5}$$

$$a = \frac{\Gamma\lambda_0^2}{4\pi c \Delta\lambda_\mathrm{D}} \,. \tag{6}$$

In the above equations, Γ is the damping constant and $\Delta\lambda_\mathrm{D}$ is the Doppler width. We adopt $\Gamma = 5.8 \times 10^8$ s^{-1} for Hα and 1.5×10^8 s^{-1} for Ca II λ8542; these are mainly from radiative damping.

Using an inversion technique, we can derive the velocity probability distribution, $P(v)$; then, through the normalization of $P(v)$, the source function, S, can be obtained. This inversion technique will be described in the next section. In our computations, we adopt $\Delta\lambda_\mathrm{D} = 0.356$ Å for Hα and 0.291 Å for Ca II λ8542, corresponding to the case of a plasma temperature $T = 10^4$ K and a micro-turbulent velocity $v_t = 10$ km s^{-1}; $\tau_0 = 300$ for Hα and 1 for Ca II λ8542, which are obtained through non-LTE computations for typical slab models corresponding to the flare on 1998 November 11 (Ding et al. 2002).

3 SCHEME OF INVERSION

Equation (1) is known mathematically as the Fredholm integral equation of the first kind, which can be rewritten as

$$g = A \cdot f \,, \tag{7}$$

where g represents the data vector of $I(\Delta\lambda)$ after proper discretization, A is the product of the discretized responsive function $i(\Delta\lambda - \frac{v\lambda_0}{c})$ and integral weight Δv, and f is the function $P(v)$

to be determined. Evidently it is an ill-posed problem. We here employ a linear regularization method (Tikhonov & Arsenin 1977; Press et al. 1995) to treat this problem. In application, the inversion technique is to minimize the sum of two functionals, which can be expressed as

$$\mid A \cdot f - g \mid^2 + \mu \mid K \cdot f \mid^2 = \text{minimum} \,, \tag{8}$$

where the first term represents the residual, χ^2, and the second is a measure of smoothness. K is a matrix dependent on the specific smoothing method. This technique thus involves a trade-off between two optimizations: agreement between data and solution (i.e., minimizing χ^2) and smoothness or stability of solution.

Equation (8) can be easily reduced to a set of linear equations

$$(A^T \cdot A + \mu H) \cdot f = A^T \cdot g \,, \tag{9}$$

where $H = K^T K$. We suppose that a piecewise quadratic function for f is a good approximation, then $(K \cdot f)$ can be represented by the central difference of the third derivative of f (Newton et al. 1995)

$$(K \cdot f)_m = f'''(v_m) = \frac{-f(v_{m-\frac{3}{2}}) + 3f(v_{m-\frac{1}{2}}) - 3f(v_{m+\frac{1}{2}}) + f(v_{m+\frac{3}{2}})}{(\Delta v)^3} \,. \tag{10}$$

From Eq. (10), we obtain the matrix K that is then substituted into Eq. (9), which can then be solved by the LU decomposition method. The ill-conditioning is thus removed through the introduction of the μ term. Application of this method can be found in some papers (e.g., Jeffrey & Rosner 1986; Newton et al. 1995). However, how to precisely define the smoothness (i.e., the value of μ) may be crucial to the solutions. To determine the value of μ, we synthesize the methods proposed by Tikhonov & Arsenin (1977), Titterington (1985), and Metcalf et al. (1990) and then impose a random perturbation on the observed profile g to acquire a new one, g_δ. The error, $\delta = \mid g_\delta - g \mid$, is a known value. We then take a finite geometric progression $\mu = \mu_0 q^k$ $(q > 0)$, for $k = 0, 1, 2, ..., n$; and select a μ that yields a solution of f_μ within the required accuracy, i.e., $\mid A \cdot f_\mu - g_\delta \mid \leq \delta$.

To test the validity of the inversion technique, we construct artificial line spectra using different velocity distributions, and then make the inversion. The velocity field can be reproduced in most cases based on this method.

4 RESULTS

We apply the method described above to actual computations. Figure 2 plots the underlying function $P(v)$ after deconvolution. Also shown are the mean velocity that is obtained by

$$\bar{v} = \int v P(v) \mathrm{d}v \,, \tag{11}$$

and the width of the velocity distribution defined as the range within which $P(v)$ lies above e^{-1} of its maximum. From Fig. 2, we can see that the half width reaches more than 150 km s^{-1} at the top of the loop for Hα, while only about 40 km s^{-1} for Ca II λ8542. The mean velocity, however, is relatively smaller: it is no more than 35 km s^{-1} for Hα and no more than 20 km s^{-1} for Ca II λ8542. Therefore, there is an apparent difference in the velocity distributions derived from Hα and Ca II λ8542. This point will be explained below. The two lines, however, share the

same type of line asymmetry, as can be seen from Fig. 2, where the average velocities determined from Hα and Ca II λ8542 have the same sign. This point can also be visually checked from the original line profiles.

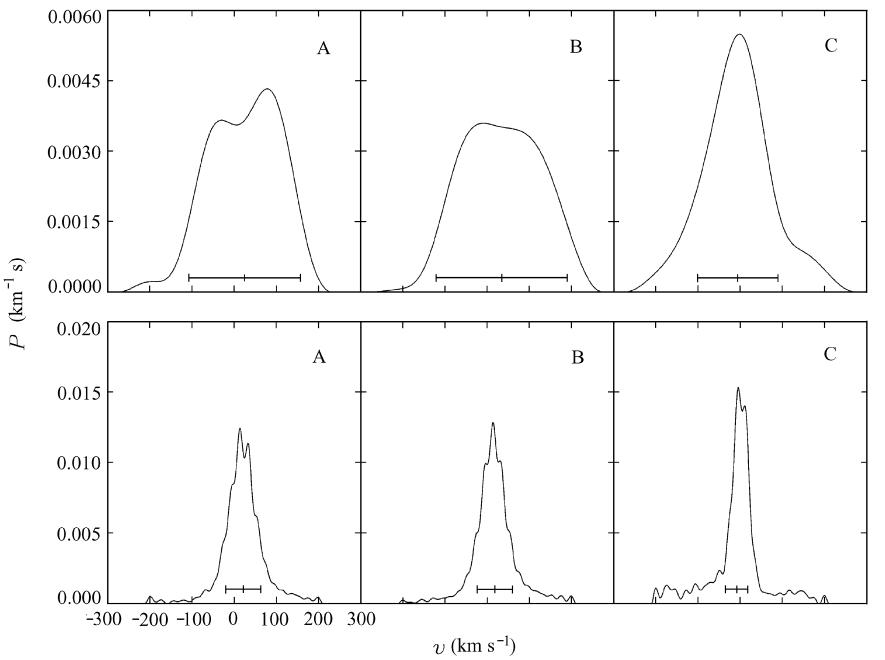

Fig. 2 Velocity probability distribution deduced from Hα (upper panel) and Ca II λ8542 (lower panel) for the three locations at 02:14:38 UT. The center of the horizontal bar in each panel represents the mean velocity; its length refers to the width of the velocity profile.

From Fig. 3, we can see that the observed line profiles are well recovered; besides, when we adopt other values for μ that depart from the optimal one, the velocity profiles do not change markedly. We have thus scored a good agreement between the original data and stable solutions. One interesting thing is that, as illustrated in Fig. 3 (left panel), we can extend the recovered profile to a wavelength window broader than that in observations. This will compensate for the disadvantage of the observed Hα profile restricted within too narrow a wavelength range. We are thus able to calculate the intensity integrated over the whole Hα line profile. As is commonly known, in the case of line broadening caused by macro-turbulence, only the line profile is broadened, while the equivalent width remains unchanged. On comparing the line integrated intensity of $i(\Delta\lambda)$ with that of the recovered profile $I(\Delta\lambda)$, we did find equality, precisely as expected.

Having acquired the velocity distribution, we then investigate the temporal variation of the half width and the source function. The results are plotted in Fig. 4. It clearly shows that the width of the velocity distribution and the source function derived from Hα are rather larger than those from Ca II λ8542. Just as stated by some authors (Heinzel & Rompolt 1987; Heinzel et al. 1992), strong turbulent broadening can significantly increase the source function of the Hα line. This point is also supported by the fact that, in the case of Hα, the width of the velocity distribution shows an evolution largely similar to that of the source function. Such

a similarity does not exist in the case of Ca II λ8542, which may indicate that the line source function of Ca II λ8542 is less affected by macro-turbulence.

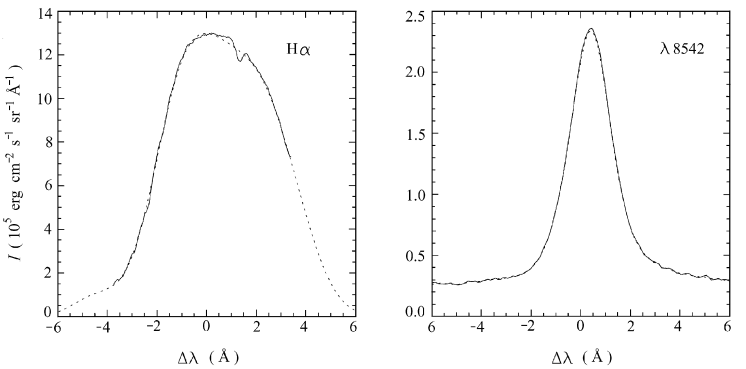

Fig. 3 Comparison between the observed line profiles (solid lines) and the profiles recovered in our method (dotted lines).

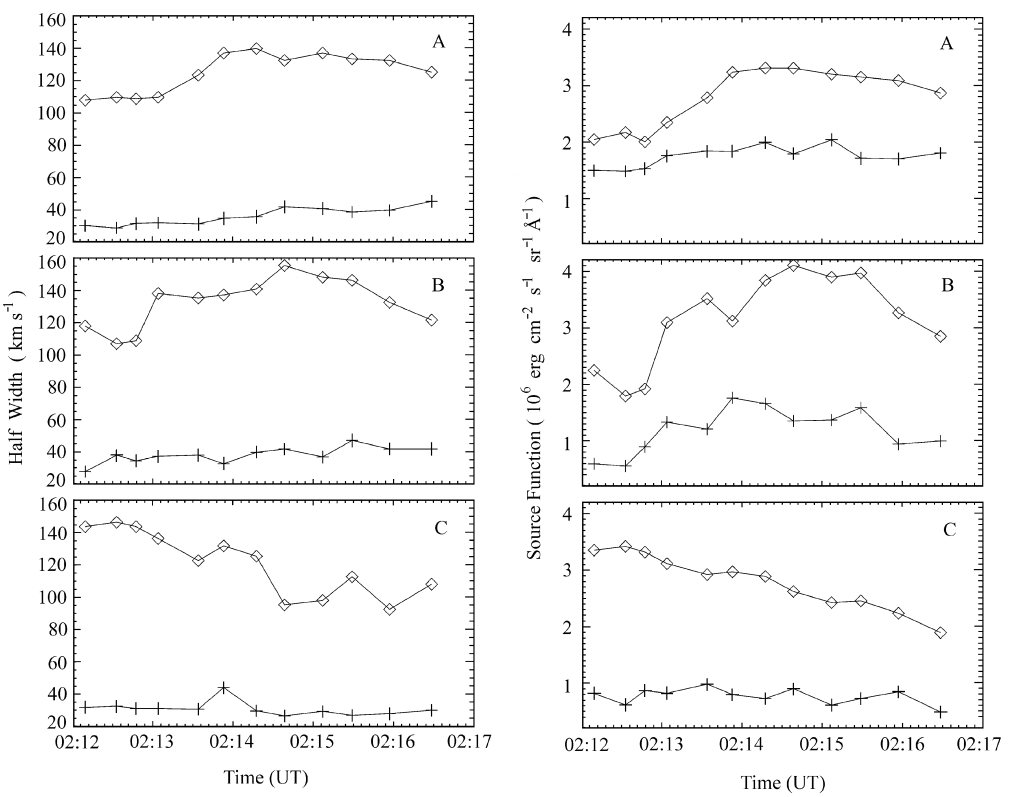

Fig. 4 Temporal variations of the half width of the velocity distribution (left panel) and the source function (right panel) for Hα (diamonds) and Ca II λ8542 (plus signs) at the three locations.

Also note that around the flare maximum (02:15 UT), the widths of the velocity distribution and the source function derived from Hα are larger at the top of the loop than in the legs, whereas this is not always so for Ca II λ8542. These facts show again the different behaviors of the physical parameters derived from the two lines. Through non-LTE computations, Ding et al. (1999) have demonstrated that Hα peaks at a higher temperature than does Ca II λ8542 (see their fig. 3). By assuming a homogeneous slab model, Ding et al. (2002) further derived the temperature at the three locations ($10000 - 12500$ K, see their fig. 6). In this temperature range, the emission of Ca II λ8542 is rather weak and decreases with temperature, contrary to the emission of Hα. We find that the source function of Hα deduced here bears an evolution trend very similar to that of the temperature, but this similarity does not hold for Ca II λ8542. This result supports the above points. As the flaring loop contains a large macro-velocity, the two lines may suffer different Doppler brightening or dimming effects as stated above, which can also change the velocity dependence of the line emission. Therefore, we propose that the main cause of the different velocities derived from Hα and Ca II λ8542 is that the emissions of the two lines depend in different ways on temperature and velocity.

From Fig. 4, we can also find that the width of the velocity distribution is kept large even in the later phase. This large scale motion can explain the excessive line broadening persisting in the later phase without invoking non-thermal effects.

5 DISCUSSION

After showing the feasibility of line broadening caused by large scale mass motions, we now discuss the possible origin of the motions. However, this key problem is rather controversial. In the present observations, the loop top is the brightest region, and the Hα line is most broadened there. Hence, any possible origin of the large scale motions should be consistent with this specific scenario. Uchida & Shibata (1988) have presented an MHD model for the heating of loop flares. In their model, an enormous mass is driven dynamically along twisted magnetic tubes into the top of the loop through the pinch effect, and then the material collides at the top. The longitudinal motion is destroyed at the collision, whereas the rotational motion is strengthened and persists even after the crash. Due to macroscopic fiction, the rotational motion may be damped and would develop into a macro-turbulence over an extended time of tens of minutes. On the other hand, if flares occur through magnetic reconnection, as is generally believed, materials will be driven as outflows from the magnetic neutral point because huge energy is released there. We can hence postulate that, if the neutral point is located above the flaring loop, the outflows will impinge on the loop top and make it significantly condensed. The macro-turbulence can also be readily induced there. The existence of such a process is verified by hard X-ray observations (Masuda et al. 1994).

It is generally believed that the cool loops visible in Hα are evolved from the cooling of the hot X-ray loops (e.g., van Driel-Gesztelyi et al. 1997). It is therefore possible that the macro-turbulence may remain in the Hα loop provided that the cooling time of the flaring loop is short enough. Here we check this point further. Ding et al. (2002) have obtained that the mass density in the flaring loop reaches about $(1 - 3.5) \times 10^{12}$ cm^{-3}. So we are able to estimate the cooling time from the hot X-ray loops to the cool Hα loops ($T < 2 \times 10^4$ K). We use the same method given by Schmieder et al. (1995, 1996, and references therein) to compute the cooling time for an initial temperature $T_0 = 10^7$ K and a semi-length $L = 2 \times 10^4$ km for the limb flare, taking into account radiative loss and thermal conduction. The plasma is assumed to

be fully ionized, which is approximately valid above temperatures around 2×10^4 K. In order to make a comparison, we consider various values of the electron density: $n_e = 10^{11}, 3 \times 10^{11}, 10^{12}$ and 3×10^{12} cm^{-3}. The results are plotted in Fig. 5.

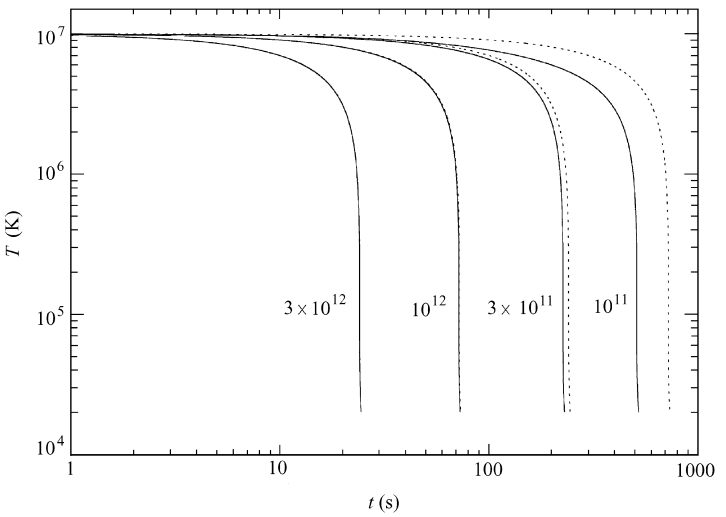

Fig. 5 Comparison of the cooling of a loop of semi-length $L = 2 \times 10^4$ km for different electron densities. Solid lines refer to cooling through both radiative loss and thermal conduction; dotted lines, radiative loss only.

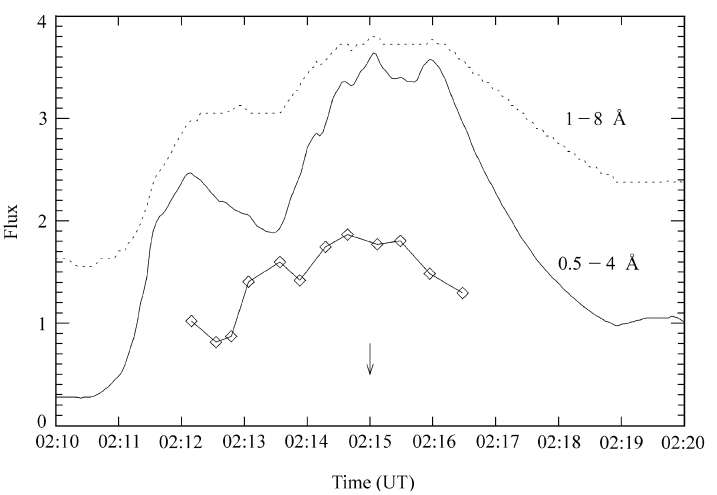

Fig. 6 Time profiles of the soft X-ray flux at $1 - 8$ Å (dotted line) and $0.5 - 4$ Å (solid line). Also plotted is the evolution of the source function of Hα (diamonds) at the location B. The arrow indicates the time of the Hα maximum. The units are arbitrary.

Examining Fig. 5, we can see that the cooling time for different electron densities is generally consistent with the results of Gan & Fang (1990, see their table 3), Švestka et al. (1987, see their sect. 3), and Schmieder et al. (1995, see their fig. 10). The cooling time is rather short for electron densities above 10^{12} cm^{-3}, i.e., no more than 30 s for $n_e = 3 \times 10^{12}$ cm^{-3} and about 1 min for $n_e = 10^{12}$ cm^{-3}. Since the loop geometry may exhibit a twisted structure, the path of thermal conduction may be greatly extended and conductive cooling may consequently become less effective. However, we can see from Fig. 5 that, in the case of a high electron density, heat conduction is negligible; that radiative loss plays the leading role in the cooling that is not much affected by the loop geometry.

Figure 6 displays the time profiles of the soft X-ray flux at $1 - 8$ Å and $0.5 - 4$ Å for this flare observed by *GOES*, as well as the temporal evolution of the source function of Hα at the location B. We can see that, within the time resolution, the flux at the two wavelength bands and the source function peak roughly simultaneously around the Hα maximum. This near simultaneity confirms the fast cooling of the flaring loop. It is thus reasonable to suppose that macro-turbulence may persist at the top of the Hα loop. In this context, the Hα line at the top of the limb flare will inevitably suffer a great broadening; the loop top is hotter, condensed (Ding et al. 2002), and accordingly has a greater source function than elsewhere.

6 CONCLUSIONS

We propose that the unusual line broadening of Hα in a limb flare on 1998 November 11 is mainly due to large scale mass motions or macro-turbulence, and use an inversion technique to deduce the velocity distribution along the line of sight. The line-of-sight velocity derived from Hα can exceed 150 km s^{-1}, whereas that from Ca II λ8542 is only about 40 km s^{-1}, which may result from the fact that the emissions of the two lines have different dependence on temperature and velocity. This point is also evidenced by different spatial distributions and temporal evolutions of physical parameters derived from Hα and Ca II λ8542 (Fig. 4).

We suggest two possible origins for the large scale motions that are invoked to account for the observed line width. The flaring loop in this event bears a high mass density and accordingly a very short cooling time (several tens of seconds); therefore, the large motions or macro-turbulence produced in the energy release process (in hot loops) can persist in the cool loops of Hα. The loop top is thus the hottest and most condensed, and it is also most turbulent there.

One may question why only limb flares possess such large inhomogeneous motions. We believe that in disk flares, similar macro-turbulence should also exist, but because, here, the emission from the flaring loop is superimposed on the background emission, it is not easy to recover the velocity field properly. Usually, the velocity deduced in disk flares is smaller than in limb flares.

Acknowledgements This work was funded by NSFC under grant 10025315, NKBRSF under grant G20000784, and by TRAPOYT.

References

Antonucci E., Gabriel A. H., Acton L. W., Culhane J. L., Doyle J. G., Leibacher J. W., Machado M. E., Orwig M. E., Raplay C. G., 1982, Solar Phys., 78, 107
Bentley R. D., Lemen J. R., Phillips K. J. H., Culhane J. L., 1986, A&A, 154, 255
Ding M. D., Fang C., Yin S. Y., Chen P. F., 1999, A&A, 348, L29
Ding M. D., Liu Y., Chen P. F., 2002, Solar Phys., in press
Emslie A. G., Alexander D., 1987, Solar Phys., 110, 295
Fang C., Hénoux J. -C., Ding M. D., 2000, A&A, 360, 702
Gan W. Q., Fang C., 1990, ApJ, 358, 328
Graeter M., Kucera T. A., 1992, Solar Phys., 141, 91
Gu X. M., Li B., Li Q., Ding Y. J., Xu A. A., Ding J. P., Tang Y. H., 1984, Scientia Sinica, XXVII 9, 973
Heinzel P., Rompolt B., 1987, Solar Phys., 110, 171
Heinzel P., Schmieder B., Mein P., 1992, Solar Phys., 139, 81
Huang Y. R., Fang C., Ding M. D., Gao X. F., Zhu Z. G., Yin S. Y., Hu J., Xue Y. Z., 1995, Solar Phys., 159, 127
Jeffrey W., Rosner R., 1986, ApJ, 310, 463
Li H., You J., 2001, A&A, 374, 1121
Malherbe J.-M., Tarbell T., Wiik J. E., Schmieder B., Frank Z., Shine R. A., van Driel-Gesztelyi L., 1997, ApJ, 482, 535
Masuda S., Kosugi T., Hara H., Tsuneta S., Ogawa Y., 1994, Nature, 371, 495
Metcalf T. R., Canfield R. C., Avrett E. H., Metcalf F. T., 1990, ApJ, 350, 463
Newton E. K., Emslie A. G., Mariska J. T., 1995, ApJ, 447, 915
Press W. H., Teukolsky S. A., Vetterling W. T., Flannery B. P., 1995, Numerical Recipes in C, Cambridge Univ. Press, Cambridge, p. 804- 812
Raju K. P., 1999, Solar Phys., 185, 311
Schmieder B., Heinzel P., van Driel-Gesztelyi L., Lemen J. R., 1996, Solar Phys., 165, 303
Schmieder B., Heinzel P., Wiik J. E., Lemen J., Anwar B., Kotrč P., Hiel E., 1995, Solar Phys., 156, 337
Švestka Z., Fontenla J. M., Machado M. E., Martin S. F., Neidig D. F., Poletto G., 1987, Solar Phys., 108, 237
Tikhonov A. N., Arsenin V. Y., 1977, Solutions of Ill-Posed Problems, Wiley, New York, p. 87
Titterington D. M., 1985, A&A, 144, 381
Uchida Y., Shibata K., 1988, Solar Phys., 116, 291
van Driel-Gesztelyi L., Wiik J. E., Schmieder B., Tarbell T., Kitai R., Funakoshi Y., Anwar B., 1997, Solar Phys., 174, 151
You J., Oertel G. K., 1992, ApJ, 389, L33
You J., Wang C., Fan Z., Li H., 1998, Solar Phys., 182, 431